Excitonic Energy Shell Structure of Self-Assembled InGaAs/GaAs Quantum Dots

S. Raymond,[1] S. Studenikin,[1] A. Sachrajda,[1] Z. Wasilewski,[1] S. J. Cheng,[1] W. Sheng,[1] P. Hawrylak,[1] A. Babinski,[2,4]
M. Potemski,[1,2] G. Ortner,[3] and M. Bayer[3]

[1]*Institute for Microstructural Sciences, National Research Council of Canada, Ottawa, Ontario K1A 0R6, Canada*
[2]*Grenoble High Magnetic Field Laboratory, MPI/FFK and CNRS, BP 166, 38042, Grenoble Cedex 9, France*
[3]*Experimentelle Physik II, Universität Dortmund, D-44221, Dortmund, Germany*
[4]*Insitute of Experimental physics, Warsaw University, Hoza 69, 00-681 Warszawa, Poland*
(Received 11 September 2003; published 6 May 2004)

Performing optical spectroscopy of highly homogeneous quantum dot arrays in ultrahigh magnetic fields, an unprecedently well resolved Fock-Darwin spectrum is observed. The existence of up to four degenerate electronic shells is demonstrated where the magnetic field lifts the initial degeneracies, which reappear when levels with different angular momenta come into resonance. The resulting level shifting and crossing pattern also show evidence of many-body effects such as the mixing of configurations and exciton condensation at the resonances.

Quantum dots have been at the heart of intense research efforts in view of both the high potential for applications as well as new physics on a nanoscale [1–3]. The basic understanding of the quantum dot (QD) properties is necessary in order to fully exploit their application potential. This fundamental understanding of QD systems is based on a knowledge of their energy shell structure and of relevant carrier interactions. To this effect, spectroscopy experiments in high magnetic fields are an appropriate probing tool. For example, Coulomb blockade spectroscopy of single, electrostatically defined QDs [4–6] has revealed a shell structure that can be understood in terms of two-dimensional harmonic oscillators, the Fock-Darwin (FD) spectrum [7,8], which is strongly modulated by a charging energy due to the injection of negatively charged electrons. Also, low-field magnetoluminescence of QD arrays [9–12] was performed, but a limited magnetic field range as compared to interlevel spacing prevented the observation of the clear crisscross pattern typical of FD diagrams. In contrast, by following the interband emission of charge-neutral electron-hole pairs in a large array of highly homogeneous self-assembled QDs subject to high magnetic fields, we directly observe the FD-like spectrum representative of the QD ensemble. From it, we show that the energy shell structure can be understood in terms of a weakly modulated FD spectrum of electron-hole pairs (excitons), where charge neutrality and high symmetry lead to subtle manifestations of many-body effects.

The InAs QD layer sample was grown by molecular beam epitaxy on a GaAs substrate, and details of the growth can be found elsewhere [13]. In view of the small QD size (~20 nm base, ~3 nm heigth), one obtains a discrete electronic energy spectrum as confirmed by previous studies on single quantum dots [14–16], where the interpretation of the state-filling spectroscopy relied on the assumption of a two-dimensional harmonic oscillator

shell structure [16]. This structure is reproduced in Fig. 1(a), where the solid (open) arrows indicate a level occupied by electrons (holes) and two-way arrows indicate dipole-allowed transitions. These transitions can be observed in the high excitation photoluminescence (PL) spectra of the QD ensemble [17], as shown in the bottom (black) curve of Fig. 1(b), where by analogy with atomistic energy levels they are labeled with letters *s, p, d, …* [16]. Altogether we observe four QD-related lines, from *s* to *f*, and one additional line associated with the wetting layer (WL), which are inhomogeneously broadened. In order to clearly resolve information on the shell structure, minimization of this broadening was achieved by optimizing the growth conditions to improve height uniformity [13] and by performing post-growth annealing [18]. Figure 1(b) shows the blueshift, reduction in transition spacing and reduction in linewidth obtained upon annealing of our sample. The observed effects are related to injection of Ga into the QDs from barrier material, which increases the QD material gap and possibly modulate their size and shape. For the highest annealing temperature, a peak spacing of 36 meV and a FWHM of 15 meV are obtained, and this highly homogeneous QD layer is the focus of our study.

The key to unambiguously determining the shell structure is the application of a magnetic field. To this effect, the emission spectrum of the QD ensemble was measured with magnetic fields up to 28 T applied perpendicular to the plane of the QDs. Figure 1(c) presents the evolution of the emission spectrum in the form of a surface plot. A clear pattern of peak splitting, shifting, and crossings is observed. The *s*-peak energy (starting energy ~1.36 eV) increases monotonously with magnetic field, as does the wetting layer emission. The *p* peak splits into two lines and the *d* peak into three. Based on this 1-2-3 splitting sequence, one would expect the *f* line to split into four branches. However, since this line is almost

degenerate with the WL, only the lower branch can be observed while the other three branches become unbound with increasing field. Conversely, a number of new lines peel off from the wetting layer continuum and converge with the s-line emission. In the process, the lower branch of the g, h, and i lines cross the upper branches of the p and d lines.

This striking pattern can be understood in simplified terms as direct observation of a FD spectrum [7,8]. The electronic energy spectrum dependence in a magnetic field is given by that of two harmonic oscillators with quantum numbers n_+ and n_-, and corresponding frequencies $\Omega_+(B)$, $\Omega_-(B)$:

$$E(n_+, n_-) = \hbar\Omega_+(B)(n_+ + 1/2)$$
$$+ \hbar\Omega_-(B)(n_- + 1/2) \qquad (1a)$$

$$\Omega_\pm(B) = \left\{\omega^2 + \left(\frac{\omega_c}{2}\right)^2\right\}^{1/2} \pm \left|\frac{\omega_c}{2}\right|;$$

$$n_+, n_- = 0, 1, 2..., \qquad (1b)$$

where $\omega_c = eB/m^*$ is the cyclotron frequency and ω is the harmonic frequency describing the strength of in-plane parabolic confinement. At zero fields, the shell structure of the FD states is that shown for the electrons in Fig. 1(a), with state index $|n_+, n_-\rangle$ given as $|0, 0\rangle$ for the ground state, $|0, 1\rangle$ and $|1, 0\rangle$ for the first excited state and so on. The degeneracy of states with different index in a given shell is lifted by the magnetic field, and secondary degenerate shells are reconstructed for magnetic fields such that $\Delta n_+ \cdot \Omega_+(B) = \Delta n_- \cdot \Omega_-(B)$. The predictions of Eqs. (1) cannot be compared directly with results from semiconductor quantum dots for which one needs to consider electrons and holes. However, for dipole-allowed transitions, only electrons and holes with the same set of quantum numbers can recombine [two-way arrows Fig. 1(a)], and one can sum electron and hole energies to form an "excitonic" FD spectrum:

$$E(n_+, n_-) = E_0 + \hbar\hat{\Omega}_+(B)(n_+ + 1/2)$$
$$+ \hbar\hat{\Omega}_-(B)(n_- + 1/2) \qquad (2a)$$

$$\hat{\Omega}_+(B) = \Omega_+^{el}(B) + \Omega_+^{hole}(B), \qquad (2b)$$

where E_0 is an offset comprising semiconductor gap and vertical confinement energy. An example of such spectrum is shown in Fig. 2(a). The splitting, shifting, and crossing pattern of Fig. 1(c) is qualitatively reproduced by this excitonic FD spectrum. For example, following the lower branch of the f line in Fig. 1(c) (dashed line), a succession of intensity peaks are seen at ~7, ~10, and ~17 T. Comparing with Fig. 2(a), these correspond to successive crossing of the $|0, 3\rangle$ with the $|2, 0\rangle$, $|1, 1\rangle$, and $|1, 0\rangle$ excitonic states, respectively.

One may wonder how this simple FD model may account, even qualitatively, for a complicated process which occurs in a solid material with complicated band structure and interacting electrons. In particular, $k * p$
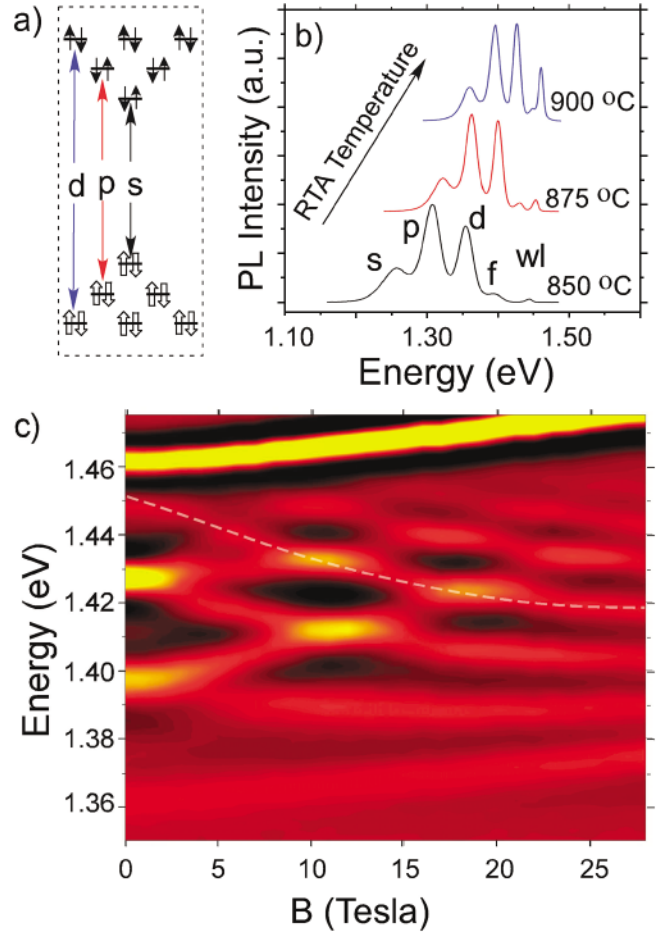
FIG. 1 (color). (a) Energy shell structure of electrons and holes for noninteracting two-dimensional harmonic oscillators (b) Emission spectra of the QD ensemble as a function of increasing annealing temperature (30 s anneals). Nominal excitation power density ~200 W/cm² (c) Surface plot describing evolution of PL (second derivative) spectrum as a function of magnetic field. Black, red, and yellow represent low, medium, and high emission intensity, respectively. Excitation power density is ~400 W/cm². All experiments performed at T = 4.2 K

and pseudopotential calculations coupled with strain calculations predict a significant splitting of the p and higher shells at $B = 0$ [19]. To address these issues we have implemented the valence band mixing within the 8-band $k * p$ model, coupled via the Bir-Pikus Hamiltonian to the strain in the dot calculated using classical elasticity theory. From the comparison of the energy of calculated and measured emission lines, we estimate the concentration of Ga in an InAs quantum dot to be ~50%. Such a significant degree of intermixing reduces shear strain and splitting of degenerate shells. The result shows that the predicted evolution is very close to the one obtained from the excitonic FD spectrum, as seen in Fig. 2(b). In particular, the crossing of all $|0, n_-\rangle$ levels with the $|1, 0\rangle$ level is well resolved.

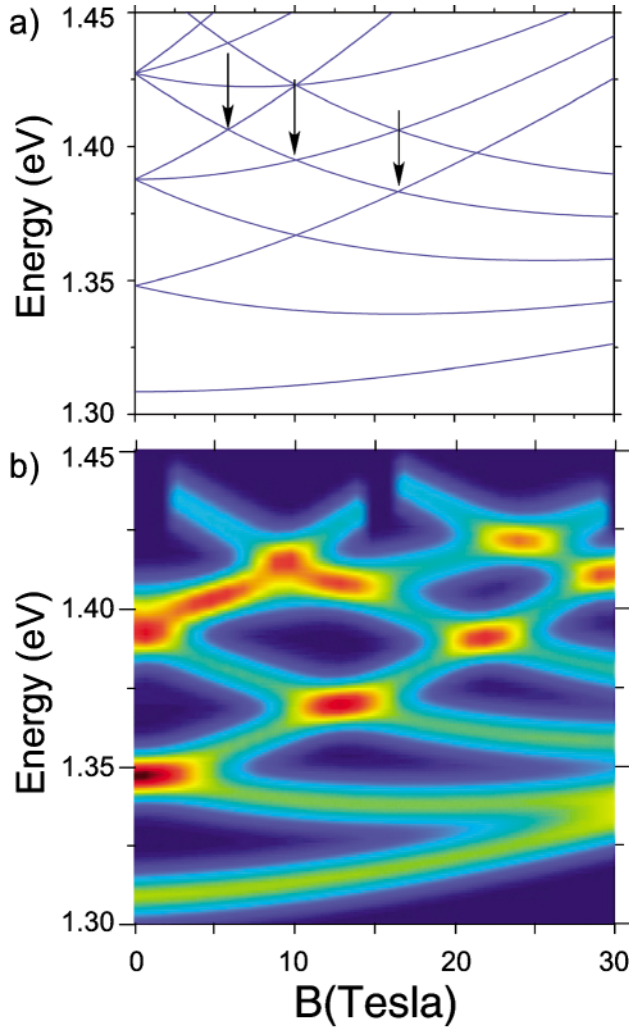Despite this strong qualitative resemblance, it is not possible to quantitatively reproduce the pattern of

FIG. 2 (color). (a) Calculated excitonic FD spectrum for electron and hole mass, confinement energy of 0.05 m_0, 0.25 m_0, 33.0 meV, and 6.6 meV, respectively. The value of E_0 was set at 1.269 for comparison with (b) calculated joint density of states from microscopic 8-band $k * p$ model.
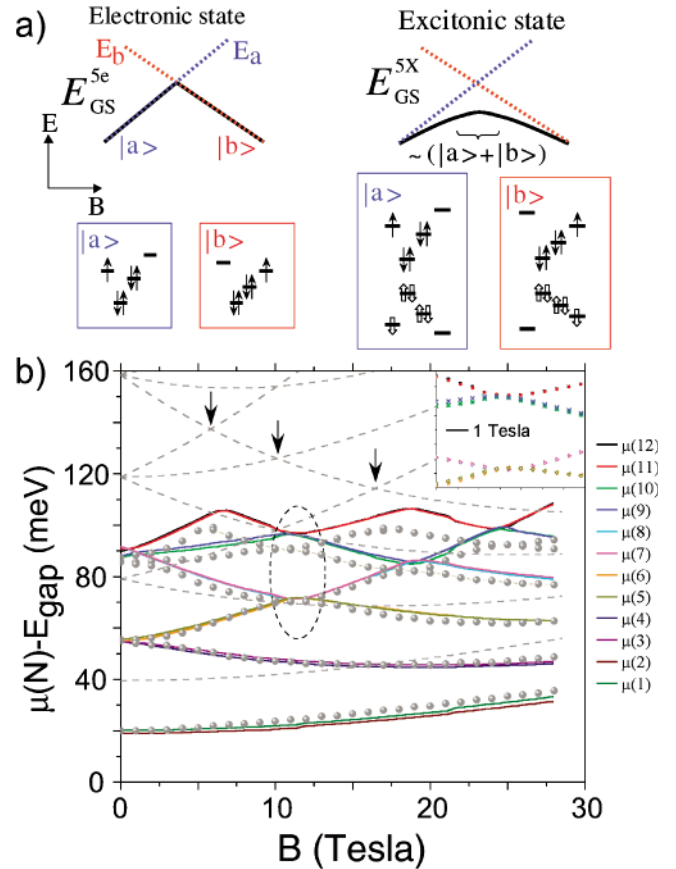

FIG. 3 (color). Calculated emission energy (chemical potential) of a quantum dot as a function of magnetic field and population of Fock-Darwin levels. (a) Difference between the evolution of five electrons versus five excitons configurations in the vicinity of crossing of FD levels. (b) Evolution of $N_X = 1 \ldots 12$ chemical potential for interacting (colored solid lines) and noninteracting (gray dashed lines) excitons. Solid circles indicate experimental peak positions, shifted in energy to have coincident $0T$ s-shell energy. Parameters used are as for Fig. 2(a) for both single-particle and many-body calculation.

transition energies of Fig. 1(c) using Eqs. (2), from which one infers the presence of many-body effects. For the sake of discussion, it is useful to introduce the chemical potential $\mu_N = E_{GS}^N - E_{GS}^{N-1}$, where E_{GS}^N is the ground state energy of a N exciton complex, or exciton droplet. The chemical potential is a convenient approximation of the emission spectrum, including many-body effects, in terms of the energy needed to add/remove an exciton from the QD. Figure 3(b) compares a noninteracting excitonic FD spectrum (dashed line), corresponding many-body calculation using chemical potential (solid lines), and experimental results (solid circles). The chemical potential was obtained from numerical calculations making use of exact diagonalisation techniques [20].

In order to discuss the many-body effects, let us examine the origin of the different contributions to the chemical potential. In a nondegenerate case, and neglecting scattering to higher shells, in the lowest order approxi-

mation only the configuration with the lowest total energy is taken into account. The chemical potential of the N-exciton dot can be expressed as

$$\mu_N = E_i^e + E_i^h - V_i^{eh} - \sum_{i \in \text{core}} V_i^{N,x}, \qquad (3)$$

where the first three terms are the energy of a single exciton consisting of the kinetic energies and the direct Coulomb attraction of the electron and hole in state i. $V_i^{N,x}$ denotes the exchange energy between the topmost particle in state N and that in a core state i. Beyond this approximation, other corrections arise from higher shell scattering and, for a degenerate shell case, from configuration coupling. The calculation shows that the latter two effects further renormalize the energy in a sense which lowers the ground state, and hence the chemical potential. The net effect of the above contributions can be observed in Fig. 3(b). At zero field, the chemical potential of the s,

p, and d shell is lowered by 20, 25, and 30 meV, respectively, due to many-body interactions. The fact that this difference becomes larger for higher shells reflects the increase in exchange energy and configuration coupling as degeneracy and number of core states increase.

Other many-body effects are related to the level crossings. For the sake of discussion, let us concentrate on the $|1, 0\rangle$-$|0, 2\rangle$ transition crossing which occurs at ~ 11 T. Let $|a\rangle$ ($|b\rangle$) denote the $|1, 0\rangle$ ($|0, 2\rangle$) state with energy increasing (decreasing) with magnetic field. Before the crossing, say, around 8 T, the $|a\rangle$ transition is described by μ_5 and μ_6 while after, say, around 14 T, it is described by μ_7 and μ_8 In between, the $|a\rangle$ and the $|b\rangle$ transitions become degenerate, and one observes an increase in intensity and a "flat region," suggesting an overlap of the transitions and a cancellation of the magnetic field dependence, respectively. These phenomena are signatures of an excitonic droplet as opposed to an electronic droplet [21,22]. For comparison, the left-hand side (right-hand side) of Fig. 3(a) shows the evolution as a function of magnetic field of the ground state energy of a five electron (exciton) system. In order to observe the crossing, we need to have four electrons (excitons) populating the two lowest levels, and at least one electron (exciton) populating the next shell. The configurations for the five electron system before ($|a\rangle$) and after ($|b\rangle$) the crossing are shown on the left-hand side of Fig. 3(a). The important point to note is that for electrons, the two configurations $|a\rangle$ and $|b\rangle$ have different total angular momenta and do not couple. Hence the electron system is in state $|a\rangle$ before the crossing and in state $|b\rangle$ after the crossing. The ground state energy of the electron droplet has a sharp cusp, which will be reflected in the evolution of the chemical potential [21,22]. For excitons, both configurations $|a\rangle$ and $|b\rangle$ involve electron-hole pairs with zero total angular momentum and hybridize. The energy of the exciton system formed averages over the energy of the two configurations which have opposite magnetic field dependence. Hence one obtains a quasivanishing magnetic field dependence at the crossing points, as shown in the inset of Fig. 3(b) and as evidenced by the flat regions in Fig. 1(c). Moreover, neglecting higher shell scattering and assuming the same wavefunction for electrons and holes (hidden symmetry condition), the chemical potential becomes independent of N for degenerate shells and one obtains an exciton condensation effect [16,20]. In other words, the charging energy involved in probing electronic systems, which in that case prevents the occurrence of clear transition crossings [22], is absent for an excitonic system. Therefore, all chemical potential curves are expected to converge towards the same energy at crossing points, where the flattened field dependence ensures that they "stick" together for a range of energy which depends on the strength of the scattering interactions, in our case a few meV.

After the crossing, the $|a\rangle$ transition has gained two extra core shell states, and now follows the evolution of μ_7 and μ_8, as compared to μ_5 and μ_6 before. This implies an extra term in the exchange energy summation of Eq. (3), which produces an offset towards lower energies. The exact diagonalization calculation gives a value of 13.2 and 16.8 meV for the direct and exchange terms of μ_5 and μ_6 at 8 T, while corresponding values of 13.3 and 21.6 meV are obtained for μ_7 and μ_8 at 14 T. This offset can be observed in Fig. 3(b), where the prolongation of the $|a\rangle$ transition on either side of the crossing does not superimpose on each other.

In conclusion, highly homogeneous QD arrays have been realized, allowing direct observation of a Fock-Darwin crisscross pattern reminiscent of charge-neutral excitons. Introducing many-body effects such as mixing of configurations, exciton condensation due to hidden symmetry, and transfer of exchange energy at crossing points, one can account for deviations from the noninteracting FD model. The observation of such fine details from the spectroscopy of large QD ensembles demonstrates the realization of highly uniform QD layers.

[1] *Nano-Optoelectronics Concepts, Physics, and Devices*, edited by M. Grundmann (Springer-Verlag, Berlin, 2002).
[2] L. Jacak, P. Hawrylak, and A. Wojs, *Quantum Dots* (Springer-Verlag, Berlin, 1998).
[3] M. Grundmann, D. Bimberg, and N. N. Ledentsov, *Quantum Dot Heterostructures*, (John Wiley & Sons Ltd., New York, 1998).
[4] P. Hawrylak, Phys. Rev. Lett. **71**, 3347 (1993).
[5] T. Fujisawa, D. G. Austing, Y. Tokura, Y. Hirayama, and S. Seigo Tarucha, Nature (London) **419**, 278 (2002).
[6] M. Ciorga *et al.*, Phys. Rev. B **61**, R16315 (2000).
[7] V. Fock, Z. Phys. **47**, 446 (1928).
[8] C. G. Darwin, Proc. Cambridge Philos. Soc. **27**, 86 (1930).
[9] P. Paskov *et al.*, Phys. Rev. B **62**, 7344 (2000).
[10] R. Rinaldi *et al.*, Phys. Rev. Lett. **77**, 342 (1996).
[11] S. Ménard *et al.*, J. Vac. Sci. Technol. B **20**, 1501 (2002).
[12] S. Raymond *et al.*, Solid State Commun. **101**, 883 (1997).
[13] Z. Wasilewski, S. Fafard, and J. P. McCaffrey, J. Cryst. Growth **201/202**, 1131 (1999).
[14] J.-Y. Marzin *et al.*, Phys. Rev. Lett. **73**, 716 (1994).
[15] M. Grundmann *et al.*, Phys. Rev. Lett. **74**, 4043 (1995).
[16] M. Bayer, O. Stern, P. Hawrylak, S. Fafard, and A. Forchel, Nature (London) **405**, 923 (2000).
[17] S. Raymond, X. Guo, J. L. Merz, and S. Fafard, Phys. Rev. B **59**, 7624 (1999).
[18] S. Fafard and C. Nì. Allen, Appl. Phys. Lett. **75**, 2374 (1999).
[19] L. W. Wang *et al.*, Appl. Phys. Lett. **76**, 339 (2000).
[20] P. Hawrylak, Phys. Rev. B **60**, 5597 (1999).
[21] M. Ciorga *et al.*, Phys. Rev. Lett. **88**, 256804 (2002).
[22] S. Tarucha, D. G. Austing, T. Honda, R. J. van der Hage, and L. P. Kouwenhoven, Phys. Rev. Lett. **77**, 3613 (1996).